Aeroacoustic Source Identification with Effects of Solid Boundaries Using a Numerical Time-reversal Technique

Yinshi Zhou, Manuel Diaz Escobar, Regis Marchiano, David Marx, Christian Prax, Vincent Valeau

AEROACOUSTIC SOURCE IDENTIFICATION WITH EFFECTS OF SOLID BOUNDARIES USING A NUMERICAL TIME-REVERSAL TECHNIQUE

Yinshi Zhou[1] **Manuel A. Diaz**[2] **Régis Marchiano**[2]
David Marx[1] **Christian Prax**[1] **Vincent Valeau** [1]
[1] Institut PPrime-UPR 3346, B17-6, rue Marcel Doré, 86022 Poitiers, France
[2] Sorbonne Université, Institut Jean Le Rond d'Alembert (UMR 7190),
4 place Jussieu, 75005 Paris, France
yinshi.zhou01@univ-poitiers.fr

ABSTRACT

Noise source identification is still a challenge in experimental aeroacoustics. For instance, traditional methods such as the beamforming technique may not give satisfactory results in presence of solid boundaries in flows, resulting from the object under study or from the experimental facility. The aim of this work is to propose an alternative strategy based on the aeroacoustic time-reversal (TR) method for the localization of sources of flow-induced noise, accounting for the solid boundaries of objects. First, a direct simulation is done to compute the radiated pressure for different sources in configurations involving solid boundaries. The base flow is supposed to be stationary and is computed with a Reynolds-averaged Navier–Stokes (RANS) solver while the pressure field is computed by solving the two-dimensional (2D) linearized Euler equations with a in house solver working with unstructured meshes. In a second step, the signals recorded on virtual microphones located on the boundaries of the domain are reversed and re-emitted in a medium where the base flow has also been reversed. First, the whole method is validated on an academic configuration. Then, localization of a synthetic dipole noise source near the trailing edge of a NACA 0012 airfoil in flow is done with a precision at wavelength.

1. INTRODUCTION

In acoustics, the TR method is known to be a robust method for sound source imaging in the ultrasonic and audible range [1]. It works in two stages. At first, sensors at the boundary of a domain of interest record the waves generated by the source; in a second step, the signals are reversed in the time domain and re-emitted by the sensors which act as sources. This phase solves the inverse problem and is carried out numerically for sound source imaging purposes.

The TR method was applied for the first time by Deneuve *et al.* for localizing aeroacoustic sources in a shear layer [2], based on numerical data. The method was also applied to experimental data for imaging artificial noise sources located in a wind-tunnel flow [3]. Several studies have applied TR to aeraocoustics since then (*eg.*, [4, 5]). The TR technique can be an alternative technique to beamforming for situations where the Green function is not known. Such situations arise when complex flow gradients are present or when solid boundaries (experimental facility, obstacles) diffract and reflect sound within the flow.

In this context, the goal of the present paper is to present a numerical methodology based on the aeroacoustic TR method for the localization of sources of flow-induced noise, accounting for the solid boundaries of objects. The numerical methods for solving the sound propagation and the mean flow are presented in Section 2, together with a validation case to assess the robustness of the acoustic solver. In Section 3, the case of a synthetic dipolar source in a flow, diffracted by a symmetric airfoil (NACA 0012) is presented, in order to approach the situation where trailing edge noise is diffracted by the airfoil, which is a significant effect when the airfoil is not acoustically compact at the emission frequency. The paper ends with a set of conclusions (Section 4).

2. NUMERICAL METHODS AND VALIDATIONS

2.1 Numerical methods for acoustic solver

In this work, aeroacoustic descriptions on stationary flows are obtained with the linearized Euler equations (LEE). In this system, the density ϱ_a, the velocity $\boldsymbol{v}_a$ and the pressure $\wp_a$ designate small perturbations superimposed on a mean flow with density ϱ_0, velocity $\boldsymbol{v}_0$ and pressure $\wp_0$. γ designates the ratio of specific heats, which is taken as γ = 1.4 for air. In a 2D domain, the LEE formulation of Bailly and Juve [6] is written in the form of a *non-conservative hyperbolic system*, namely

$$\boldsymbol{q}_t + \boldsymbol{F}(\boldsymbol{q})_x + \boldsymbol{G}(\boldsymbol{q})_y + \boldsymbol{M}_0\boldsymbol{q} = \boldsymbol{S}(t)\,\boldsymbol{\delta}(\boldsymbol{x}) \qquad (1)$$

where the vector of quantities and associated fluxes read

$$\boldsymbol{q} = \begin{bmatrix} \varrho_a \\ u_a \\ v_a \\ \wp_a \end{bmatrix}, \quad \boldsymbol{F}(\boldsymbol{q}) = \begin{bmatrix} \varrho_a u_0 + \varrho_0 u_a \\ u_0 u_a + \wp_a \varrho_0^{-1} \\ u_0 v_a \\ u_0 \wp_a + \gamma \wp_0 u_a \end{bmatrix}, \quad \boldsymbol{G}(\boldsymbol{q}) = \begin{bmatrix} \varrho_a v_0 + \varrho_0 v_a \\ v_0 u_a \\ v_0 v_a + \wp_a \varrho_0^{-1} \\ v_0 \wp_a + \gamma \wp_0 v_a \end{bmatrix}, \qquad (2a)$$

while the product $\boldsymbol{M}_0\boldsymbol{q}$, that represents the corrections induced by the variations (the inhomogeneities) in the mean flow, explicitly reads

$$\boldsymbol{M}_0\boldsymbol{q} = \begin{bmatrix} 0 \\ -u_a\frac{\partial v_0}{\partial y} + v_a\frac{\partial u_0}{\partial y} + (\wp_a\frac{\partial \varrho_0}{\partial x} - \varrho_a\frac{\partial \wp_0}{\partial x})\varrho_0^{-2} \\ v_a\frac{\partial v_0}{\partial x} - u_a\frac{\partial u_0}{\partial x} + (\wp_a\frac{\partial \varrho_0}{\partial y} - \varrho_a\frac{\partial \wp_0}{\partial y})\varrho_0^{-2} \\ (\gamma-1)(\wp_a(\frac{\partial u_0}{\partial x} + \frac{\partial v_0}{\partial y}) - u_a\frac{\partial \wp_0}{\partial x} - v_a\frac{\partial \wp_0}{\partial y}) \end{bmatrix}. \tag{2b}$$

Lastly, the right hand side of Eq. (1) denotes unsteady source terms that introduce a series of signals $\boldsymbol{S}(t)$ at discrete locations of the domain with the help of the Dirac delta function $\boldsymbol{\delta}(\boldsymbol{x}) = \delta(x)\delta(y)$. Here, the vector $\boldsymbol{S}(t)$ denotes mass-, force- and pressure-signal as follows

$$\boldsymbol{S}(t) = \left[S^{\rho}(t),\, S^{f_x}(t),\, S^{f_y}(t),\, S^{\wp}(t),\right]^T, \tag{3}$$

where the terms $\{S^{\rho},\, S^{f_x},\, S^{f_y},\, S^{\wp}\}$ are time-harmonic functions that, similarly to [6], can be tuned to model a monopolar or dipolar disturbance inside the physical domain.

The form of system (1) is suitable so that its acoustic fields can be discretized over a domain partitioned in K non-overlapping triangular elements as

$$\Omega = \bigcup_{k=1}^{K} \Omega^k. \tag{4}$$

To solve (1) over this partitioned domain, a weak (integral) formulation of the LEE system is considered. Such formulation can be obtained by multiplying the system (1) by a test function and integrating over the subdomain of every k-element. Then, with the help of the divergence theorem, terms that control the volume and face data are obtained. At this point, the nodal discontinuous Galerkin (DG) formulation [7] is introduced by constructing a Lagrangian basis on each triangle. This introduces internal resolution and matrix-operators that allows us to control the acoustic fields inside every element, $\boldsymbol{q}^k$, systematically. At this point, the evolution of LEE system (1) inside a every k-element is described by the semi-explicit scheme

$$\begin{aligned} \frac{\partial \boldsymbol{q}^k}{\partial t} =& \frac{\partial \xi}{\partial x}(\mathcal{M}_{ij}^R)^{-1}\mathcal{S}_{ij}^{R,\xi}\boldsymbol{F}^k + \frac{\partial \eta}{\partial x}(\mathcal{M}_{ij}^R)^{-1}\mathcal{S}_{ij}^{R,\eta}\boldsymbol{F}^k \\ &+ \frac{\partial \xi}{\partial y}(\mathcal{M}_{ij}^R)^{-1}\mathcal{S}_{ij}^{R,\xi}\boldsymbol{G}^k + \frac{\partial \eta}{\partial y}(\mathcal{M}_{ij}^R)^{-1}\mathcal{S}_{ij}^{R,\eta}\boldsymbol{G}^k \\ &- \frac{J^{\partial k}\mathcal{M}_{ij}^{\partial R}}{J^k\mathcal{M}_{ij}^R}\{(\boldsymbol{n}\cdot\boldsymbol{f})^k\}^* - \boldsymbol{M}_0^k\boldsymbol{q}^k \\ &+ (\mathcal{M}_{ij}^R)^{-1}\boldsymbol{S}(t)\boldsymbol{l}(\boldsymbol{\xi}_0). \end{aligned} \tag{5}$$

Where $\mathcal{M}_{ij}^R$ is the *reference element* mass matrix, $\mathcal{S}_{ij}^{R,\xi}$ and $\mathcal{S}_{ij}^{R,\eta}$ are the *reference element* stiffness matrices and $\mathcal{M}_{ij}^{\partial R}$ is the *reference element* mass matrix of all faces in the element. $J^{\partial k}$ and J^k are the Jacobians operators for the face and volume data, respectively. They help to map the operators from the reference frame (ξ, η) back into the physical domain (x, y). $\boldsymbol{l}(\boldsymbol{\xi}_0)$ denotes the Lagrangian base function evaluated at $\boldsymbol{\xi}_0 = (\xi_0, \eta_0)$ that corresponds to the position of the point source in the reference element. Lastly $\{(\boldsymbol{n}\cdot\boldsymbol{f})^k\}^*$ denotes numerical flux between elements faces. Here, we simply refer to [7] for their definitions.

Associating Eq. (5) with an explicit fourth-order Runge-Kutta scheme and a basis function of degree three (N=3 in the notation of [7]) results in a consistent 4th-order numerical scheme (in space and time) suitable for describing the evolution of acoustic fields. This algorithm was coded in C++ and was extended to use MPI in order to make the most out of the parallel properties of Eq. (5). Lastly, we supply this algorithm with capabilities for handling reflective and non-reflective boundary conditions. This results in an excellent framework for simulating the aeroacoustic propagation of discrete disturbances.

2.2 RANS simulation

The computation of the mean flow around objects in this work is a RANS simulation, using the open source software OpenFOAM. The turbulence model used for the simulation is k-ω SST. The mean flow flow is considered as stationary, and serves as the input data for the acoustic solver. This work deals with the case of the flow of air around a NACA 0012 airfoil with a chord of 0.2 m at an angle of attack of 10° and an incoming velocity of 39.2 m/s. The chord-based Reynolds number is 5×10^5. Unstructured mesh was used for the simulation with a prism layer mesh around the airfoil surface to account for the wall-bounded flows. The computation is conducted in parallel using 40 processors on a cluster. The y+ values and the convergence of the simulation were checked. In order to validate the numerical results, the lift coefficient of the airfoil at these conditions were computed. They were compared with the published experimental results of Ref. [8], which is shown in Tab. 1. It is found that the error of the numerical result with respect to the experimental one is less than 5%.

Data source	Lift coefficient
Simulation	0.93
Experiment [8]	0.948±0.049

Table 1. Comparison of the lift coefficients of the NACA 0012 airfoil at an angle of attack of 10° and a chord-based Reynolds number of 5×10^5.

The acoustic solver and the software OpenFOAM use different meshes. In order to map the mean flow data to the grid of the mesh of the acoustic solver, interpolation of the data between the two meshes was conducted. It is based on a cubic interpolation using a MATLAB function. Fig. 1 shows the mean flow data around the airfoil on the grid of the acoustic mesh after interpolation. The zone near the leading edge of the airfoil contains the flow with velocities lower than that of the incoming flow. The zone on the suction side and near the leading edge of the airfoil was subjected to velocities higher than that of the incoming flow. The wake of the airfoil was also observed. This corresponds well to the subsonic flow characteristics around

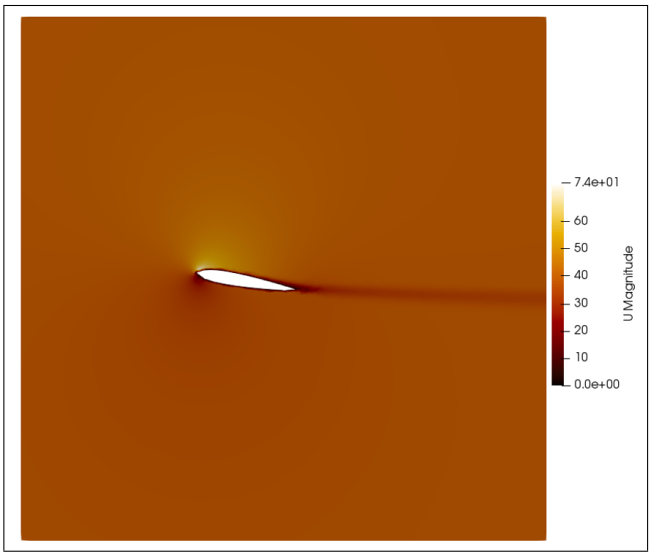

Figure 1. Mean flow field around the airfoil NACA 0012 on the grid of the mesh of the acoustic solver.

an airfoil with low angle of attack. The mean flow data can therefore be used for the acoustic solver.

2.3 Validation of the acoustic solver

A bechmark problem concerning an acoustic scattering by a cylinder [9] in a quiescent medium was revisited using the acoustic solver. The correct analytical solution of the problem was provided by Ref. [10]. The interest of this case is to check if the interaction between the sound wave and the boundaries is well solved by the acoustic solver. The domain of simulation is a square of dimensions 20 m $\times$ 20 m. The sound speed is 1 m/s. The density of the medium is 1 kg/m^3. An acoustic pulse with a Gaussian distribution in space was initially placed at the right side of the cylinder with a distance of 4 m from the center of the cylinder. The diameter of the cylinder is 1 m. Fig. 2 shows the unstructured acoustic mesh for the numerical simulation, which is more refined for the mesh elements closer to the cylinder. The mesh was decomposed into 80 partitions for the parallel computation, which are shown using different colors. A polynomial order of 3 was used for the nodal DG method. Three recording points were placed around the cylinder with a distance of 5 m from its center. Free boundary conditions were imposed at the boundaries of the domain for the simulation.

Fig. 3 shows a snapshot of the sound pressure field during the propagation of the acoustic pulse. Compared to the previously published numerical result [9] on the same test case, the propagation of the acoustic pulse was well simulated. Several wave fronts were observed. The wavefront shown by the large circle with high intensity in Fig. 3 corresponds to the direct propagation. A part of the wavefront was reflected by the cylinder, which generated the wavefronts shown by the smaller circles with lower intensity. As the free boundary conditions were imposed, no significant reflection of the sound wave was observed at the right part of the domain.

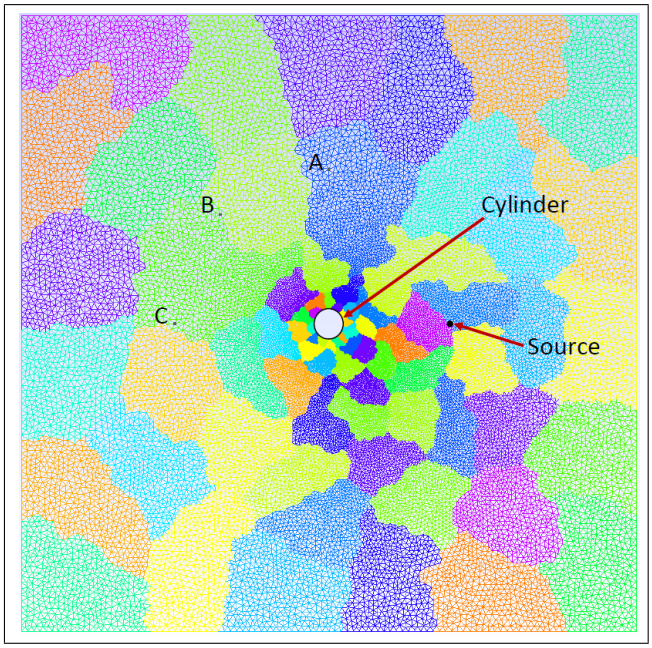

Figure 2. Unstructured mesh around a cylinder with 80 partitions for the acoustic solver.

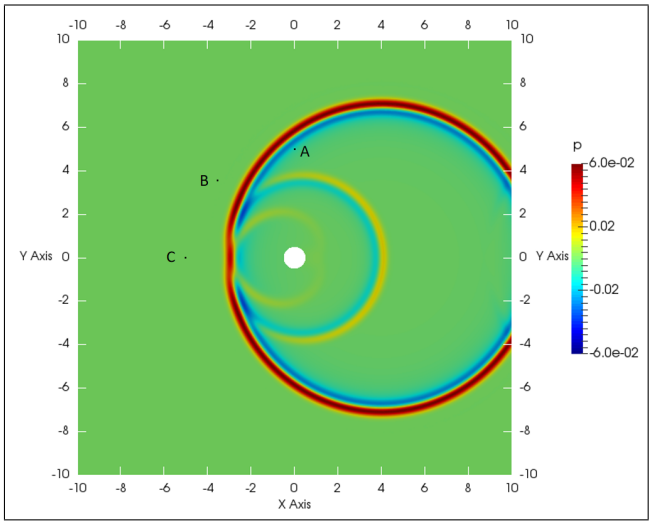

Figure 3. Snapshot of the sound pressure field for the scattering of an acoustic pulse off a cylinder.

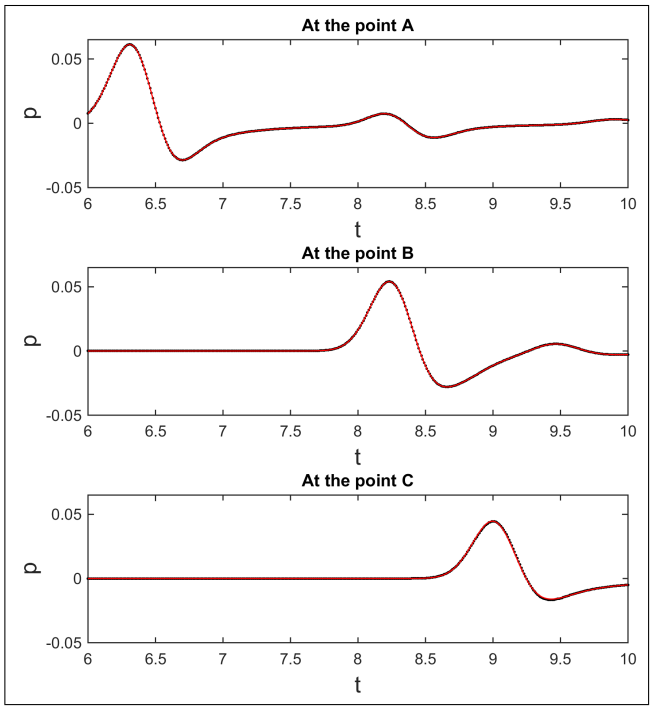

Figure 4. Comparison between the analytical and numerical results. Red lines stand for numerical simulations. Black points stand for analytical solutions.

Fig. 4 shows the sound pressure signals recorded at the three points A, B and C by red lines. They are compared to analytical results which were indicated by black points. The numerical and analytical results superimpose well for the signals at the three points. Therefore, the acoustic solver is validated for the interaction between a sound wave and solid boundaries in a 2D case using parallel computation.

3. RESULTS

This section deals with the identification of a synthetic dipole source in the mean flow field presented in the subsection 2.2. Therefore, the solid boundaries of the airfoil were considered by the RANS simulation and the simulation using the acoustic solver. As mentioned in the introduction section, this case is considered to model the diffraction of trailing edge noise by the boundaries of the airfoil. In the first step, the direct simulation was conducted. Fig. 5 shows a snapshot of the sound pressure field in the computation domain during the sound wave propagation. The dimensions of the domain is 1 m $\times$ 1 m. The sound speed is 340 m/s. The medium was considered to be air with a density of 1.2 kg/m^3. The synthetic dipole source was simulated near the trailing edge of the airfoil. Its orientation is perpendicular to the incoming flow direction (see Fig. 5). The frequency of the dipole source is 3400 Hz with a wavelength of 0.1 m. Unstructured mesh was prepared for the acoustic solver. A polynomial order of 3 was used for the nodal DG method. At each edge of the square domain, 32 isolated sets of nodes, acting as 32 uniformly distributed virtual microphones, recorded the

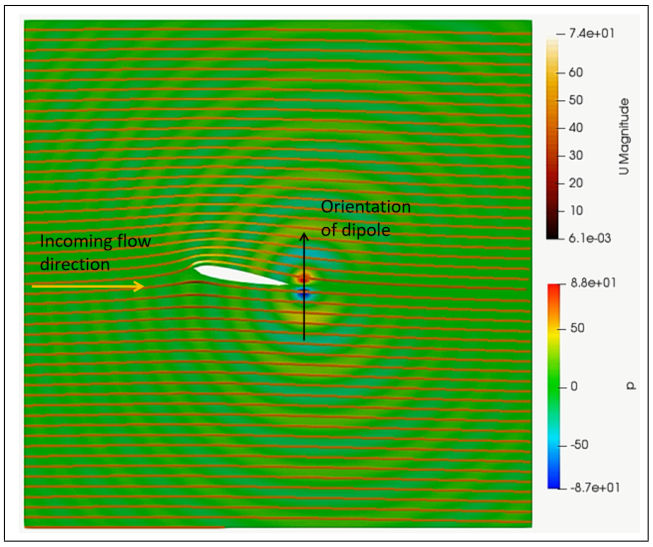

Figure 5. Result of the direct simulation of a synthetic dipole source near the trailing edge of the airfoil. The lines inside the domain are streamlines based on the stationnary mean flow.

sound pressure signals at the boundaries. Free boundary conditions were imposed at the boundaries of the domain for the simulation. The simulation time is long enough for the microphones to record non-zero data.

The second step is the TR process, the signals recorded at the boundaries were reversed and re-emitted at the same position as monopole sources. The amplitudes of the signals were all multiplied by 2 because only half of the re-emitted energy goes inside the domain. Meanwhile, the direction of the mean flow around the airfoil must also be reversed to ensure that LEE are invariant with time inversion [2, 3]. The same mesh was used but no source was simulated in the domain. Fig. 6 shows that even though not all the energy getting out of the domain were used for the TR process with a loss of information, wavefronts were still established and propagated as convergent waves in the domain. They finally collapsed at the position of the synthetic dipole source and formed two dominant spots with inverse phases, which indicates the existence of a dipole with a precision at wavelength (see Fig. 6). Note that the convergent wave continued to propagate as a divergent wave after collapsing, and it interfered with the convergent waves. Therefore, the size of the focalization spot is larger with respect to that of the direct simulation. This was reported in the work of [11] as focusing limitation of TR process. To improve the spatial resolution of the TR result, methods like acoustic sinks [12] could be used.

4. CONCLUSIONS

This work presented a numerical TR technique for noise source identification in flows by taking into account the effects of solid boundaries on wave propagation. It involves both stationary mean flow simulation around objects and sound wave propagation simulation. The technique is based on an acoustic solver which resolves LEE

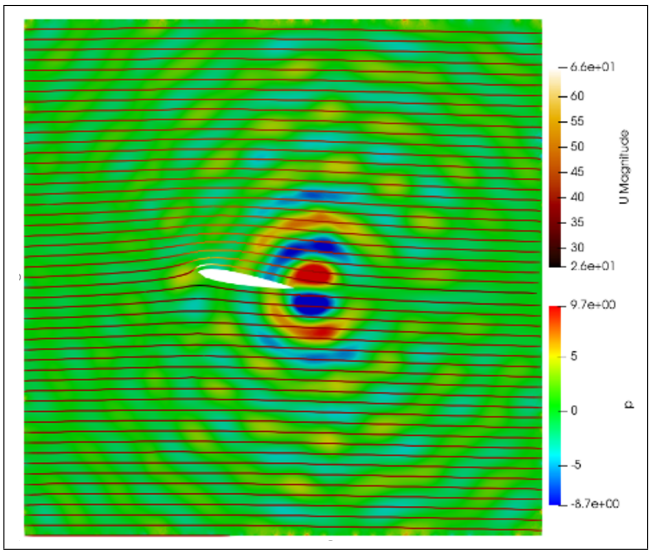

Figure 6. Result of TR of a synthetic dipole source near the trailing edge of the airfoil. The lines inside the domain are streamlines based on the stationnary mean flow.

using the nodal DG method and requires the mean flow field as input data. The acoustic solver was first validated in terms of the interaction between sound wave and solid boundaries using parallel computation. To conduct the numerical TR process, signals recorded at the boundaries were reversed in the time domain, and the stationary mean flow was reversed in space. The reversed signals and mean flow served both as input data for the acoustic solver, which allowed the numerical TR process. As a first application, the numerical TR technique can identify a synthetic dipole source in the wake of an airfoil in terms of position with a precision at wavelength.

5. ACKNOWLEDGEMENTS

The authors warmly acknowledge Jean-Christophe Vergez for his invaluable technical support. This work is supported by Agence Nationale de la Recherche (ANR) and China Scholarship Council.

6. REFERENCES

[1] M. Fink, D. Cassereau, A. Derode, C. Prada, P. Roux, M. Tanter, J.-L. Thomas, and F. Wu, "Time-reversed acoustics.," *Rep. Prog. Phys.*, vol. 63, pp. 1933–1995, 2000.

[2] A. Deneuve, P. Druault, R. Marchiano, and P. Sagaut, "A coupled time-reversal/complex differentiation method for aeroacoustic sensivity analysis: towards a source detection procedure.," *J. Fluid Mech.*, vol. 642, pp. 181–212, 2009.

[3] T. Padois, C. Prax, V. Valeau, and D. Marx, "Experimental localization of an acoustic sound source in a wind-tunnel flow by using a numerical time-reversal technique.," *J. Acoust. Soc. Am.*, vol. 132, pp. 2397–2407, 2012.

[4] A. Mimani, J. C. Doolan, and P. R. Medwell, "Multiple line arrays for the characterization of aeroacoustic sources using a time-reversal method.," *JASA Express Letters*, vol. 134, pp. 327–333, 2013.

[5] A. Mimani, D. Moreau, Z. Prime, and C. Doolan, "Enhanced focal-resolution of dipole sources using aeroacoustic time-reversal in a wind tunnel," *Mechanical Systems and Signal Processing*, vol. 72-73, pp. 925–937, 2016.

[6] C. Bailly and D. Juve, "Numerical solution of acoustic propagation problems using linearized euler equations," *AIAA journal*, vol. 38, no. 1, pp. 22–29, 2000.

[7] J. S. Hesthaven and T. Warburton, *Nodal discontinuous Galerkin methods: algorithms, analysis, and applications*. Springer Science & Business Media, 2007.

[8] C. C. Critzos, H. H. Heyson, and R. W. Boswinkle Jr, "Aerodynamic characteristics of naca 0012 airfoil section at angles of attack from 0 degrees to 180 degrees," tech. rep., National Aeronautics and Space Administration, Washington DC, 1955.

[9] C. K. Tam and J. C. Hardin, "2nd computational aeroacoustics (caa) workshop on benchmark problems," 1997.

[10] C. K. Tam, *Computational aeroacoustics: a wave number approach*, vol. 33. Cambridge University Press, 2012.

[11] D. Cassereau and M. Fink, "Time-reversal of ultrasonic fields. iii. theory of the closed time-reversal cavity," *IEEE transactions on ultrasonics, ferroelectrics, and frequency control*, vol. 39, no. 5, pp. 579–592, 1992.

[12] E. Bavu, C. Besnainou, V. Gibiat, J. de Rosny, and M. Fink, "Subwavelength sound focusing using a time-reversal acoustic sink," *Acta Acustica United with Acustica*, vol. 93, no. 5, pp. 706–715, 2007.